

One Small Step for *Roman*; One Giant Leap for Black Holes

ANDREW GOULD^{1,2}

¹*Department of Astronomy, Ohio State University, 140 W. 18th Ave., Columbus, OH 43210, USA*

²*Max-Planck-Institute for Astronomy, Königstuhl 17, 69117 Heidelberg, Germany*

ABSTRACT

The *Roman* microlensing program can detect and fully characterize black holes (BHs) that are in orbit with about 30 million solar-type and evolved stars with periods up to the mission lifetime $P \lesssim T \sim 5$ yr, and semi-major axes $a \gtrsim 0.2$ au, i.e., $P \gtrsim 10$ d $(M/M_\odot)^{-1/2}$, where M is the BH mass. For BH companions of about 150 million later (fainter) main-sequence stars, the threshold of detection is $a \gtrsim 0.2$ au $\times 10^{(H_{\text{Vega}} - 18.5)/5}$. The present *Roman* scheduling creates a “blind spot” near periods of $P \sim 3.5$ yr due to a 2.3 year gap in the data. It also compromises the characterization of BHs in eccentric orbits with periods $P \gtrsim 3$ yr and peribothra within a year of the mission midpoint. I show that one can greatly ameliorate these issues by making a small adjustment to the *Roman* observing schedule. The present schedule aims to optimize proper motion measurements, but the adjustment proposed here would degrade these by only 4–9%. For many cases of $P \gtrsim 90$ d BHs, there will be discrete and/or continuous degeneracies. For G-dwarf and evolved sources, it will be straightforward to resolve these by radial-velocity (RV) follow-up observations, but such observations will be more taxing for fainter sources. Many BH-binaries in orbits of $5 \text{ yr} \lesssim P \lesssim 10 \text{ yr}$ will be reliably identified as such from the *Roman* data, but will lack precise orbits. Nevertheless, the full orbital solutions can be recovered by combining *Roman* astrometry with RV followup observations. BH binaries with periods $10 \text{ yr} \lesssim P \lesssim 95 \text{ yr} (M/10M_\odot)^{1/4}$ can be detected from their astrometric acceleration, but massive multi-fiber RV monitoring would be needed to distinguish them from the astrophysical background due to stellar binaries.

Subject headings: gravitational lensing: micro

1. Introduction

To date, a total of four quiescent stellar-mass black holes (BHs) are known, one that is actually isolated (Sahu et al. 2022; Lam et al. 2022; Mróz et al. 2022), and three found from

Gaia observations of stars that orbit the BHs in relatively wide ($1.5 \text{ au} \lesssim a \lesssim 17 \text{ au}$) orbits (El-Badry et al. 2023a,b; Gaia Collaboration et al. 2024).

This handful of detections already clearly suggests that BH characteristics are a strong function of environment. For example, three of the four BHs have masses of $\mathcal{O}(10 M_\odot)$, local kinematics, and (for the two with measured abundances) slightly subsolar metallicities, while the fourth has $M = 33 M_\odot$, halo kinematics, and $[\text{Fe}/\text{H}] = -2.56$.

Hence, by probing BHs toward and in the Galactic bulge, one would likely gain new insights into these objects.

High-cadence, high-precision long-duration (i.e., microlensing-style) observations of the Galactic bulge permit two channels to discover and characterize BHs. The first is to detect these BHs as lenses (Gould & Yee 2014). The microlensing light curve then directly yields the so-called “microlens parallax” π_E . To extract the BH mass, $M = \theta_E/\kappa\pi_E$ (where $\kappa = 8.14 \text{ mas}/M_\odot$), one must also measure the Einstein radius, θ_E . Gould & Yee (2014) proposed that θ_E could be measured from astrometric microlensing (Walker 1995; Hog et al. 1995; Miyamoto & Yoshii 1995) from the survey itself, and this was further explored by Gould et al. (2023). However, Gould (2023) argued that while this technique could work well for BHs in the disk (along the line of sight to bulge sources), it would be very challenging for bulge BHs because both π_E and θ_E tend to be small. Regarding π_E , Gould (2023) argued that solar-orbiting-satellite microlens parallaxes (rather than annual parallax) would be needed to robustly measure π_E for most bulge BHs. Regarding θ_E , he argued that interferometric resolution of the lens images (Delplancke et al. 2001; Dong et al. 2019; Cassan et al. 2022) would be needed.

Regardless of whether bulge BHs can be detected as lenses, the same surveys open the possibility of a second channel: BHs detected from the astrometric motions of stars that orbit them. Assuming that the photon-limited statistics that were analyzed by Gould et al. (2015) for *Roman* can be achieved, then it will be straightforward to detect and characterize such BH-star systems with periods $10 \text{ d} \lesssim P \lesssim T = 5 \text{ yr}$, down to $H_{\text{Vega}} \sim 18.5$ (i.e., G dwarfs). Here $T = 5 \text{ yr}$ is the nominal lifetime of the mission. More precisely, the short period limit is set by a minimum semi-major axis $a \gtrsim 0.2 \text{ au}$, (so, $P \sim 10 \text{ d} (M/10 M_\odot)^{-1/2}$) at which point, the source orbital motion will have an amplitude that is only five times smaller than its parallax, which latter will be measured with 50σ precision. The long-period limit is set by the need to confidently measure P and a , from the astrometric data from the $T = 5 \text{ yr}$ mission. If P and a are known, then the mass function $M_* = M_\odot [(a/\text{au})^3 / (P/\text{yr})^2]$, and any value of M_* that is more than a few M_\odot will clearly be a BH. BHs can also be detected in orbit with fainter stars but with a lower limit $a \gtrsim 0.2 \text{ au} \times 10^{(H_{\text{Vega}} - 18.5)/5}$ due to reduced signal-to-noise ratio (SNR).

Unfortunately, the present *Roman* observing strategy is comprised of two reasonably well covered intervals, each lasting ~ 1.2 years, that are separated by a gap of ~ 2.3 years. This artificially-induced gap compromises the detection of a relatively broad range of periods centered on $P = 3.5$ yr. That is, at exactly $P = 3.5$ yr, the two 1.2 yr intervals cover exactly the same phase of the orbit, greatly reducing the strength of the signal (so, chance that the system will be detected) and rendering orbit reconstruction much more difficult.

According to reliable rumor mills, the densely covered *Roman* microlensing seasons (each $\Delta t = 72$ d, with about 90 observations per day), may be supplemented with the 4 remaining “off-seasons” being thinly covered (once per day). Relative to the relevant periods $P \sim 3.5$ yr, these off-seasons are short, $\Delta t/P \sim 6\%$ and so for present purposes can be considered as a single point, with error bar $\sigma = \sigma_0/\sqrt{\Delta t/d} \sim 60$ μ as, where $\sigma_0 \sim 500$ μ as is the precision at $H_{\text{Vega}} = 18.5$. This compares to an angular semi-major axis $a/D_s \simeq a/R_0 = 620$ μ as $(M/10M_\odot)^{1/3} (P/3.5 \text{ yr})^{2/3}$. Four such 10σ measurements over the 2.3 yr “gap” in the main survey would almost certainly resolve the gap-induced degeneracies. However, as this adjustment has not yet been adopted, I will ignore these extra observations in what follows. The utility of my proposed revision should ultimately be assessed in the context of the full observing strategy. Note, in particular, that the advantages of my revised observing schedule for detecting BH-binaries in very wide orbits, $P \lesssim 100$ yrs, are not affected by the incorporation (or lack thereof) of additional low-cadence observations. See Sections 6 and 7.

2. Proposed Modification to the Observing Schedule

I model the *Roman* observations as taking place during $m = 6$ campaigns, each centered on an equinox, each consisting of $n \gg 1$ observations that are uniformly distributed over a total time of $\Delta t = 72$ d. That is, the observations are at times $t_{i,j}$

$$t_{i,j} = \tau_i + \delta\tau_j, \quad \delta\tau_j \equiv \frac{j}{n}\Delta t; \quad (-n/2 < j < n/2). \quad (1)$$

Note that there are a total of $N = nm$ observations. I advocate the following change for the six τ_i

$$\begin{pmatrix} \tau_i^{\text{Roman}} \\ \tau_i^{\text{Gould}} \end{pmatrix} = \begin{pmatrix} -9 & -7 & -5 & +5 & +7 & +9 \\ -9 & -7 & -1 & +1 & +7 & +9 \end{pmatrix} Q; \quad Q \equiv \frac{\text{yr}}{4}. \quad (2)$$

The main reason for the change is to remove artificial gaps in the sensitivity to BHs, but it does have other implications, which must be addressed. Figure 1 shows the largest phase-gap as a function of period under the two strategies. The current *Roman* strategy is plotted in black and my (Gould) strategy is plotted “on top” of this in red. Because the two

curves perfectly overlap in some regions, I replot the *Roman* strategy on the very top, but with much sparser sampling and slightly larger points.

Figure 1 shows that there are five features that the two strategies have strictly in common. First, there are no gaps for $P < 72$ days because each strategy is composed of six 72-day continuous seasons. Second, there is a nearly triangular peak of 218° at $P = 0.5$ yr and with a base of 25 days. At the peak period, each season covers exactly the same range of phases, and thus always contains the intra-equinox gap of 110.5 days, corresponding to 218° . Both strategies cover the first and last available equinoxes, so in either case, as P deviates from exactly 0.5 yr, the last season moves relative to the first to progressively cover the gap. Third, there is another nearly triangular peak of 109° at $P = 1$ yr (i.e., exactly twice the previous one) and with a base of 64 days. The reason behind this is almost identical, but applied to the fact that both strategies observe the first two and last two equinoxes. The largest gap is still the one between two successive seasons, but this corresponds to half the angle. Fourth, there is yet another peak at $P = 0.25$ yr, but this has a base of only 2 days and so has no practical significance. Finally, at long periods, $P > 7$ years, the two strategies have the same rising gap size. This is because they both cover the first and last equinoxes, so the largest gap is simply $(P - 4.7)$ yr in both cases.

The two strategies also have two features that are qualitatively very similar. First, each contains two triangular features with peaks of $\mathcal{O}(120^\circ)$ between $P = 0.4$ yr and $P = 0.67$ yr (in addition to the one at $P = 0.5$ yr). Second, they have a series of structures of height $\mathcal{O}(75^\circ)$ between $P = 0.7$ yr and $P = 1.6$ yr (in addition to the one at $P = 1$ yr). For the *Roman* strategy, these are a set of regular peaks, while for the Gould strategy, they are irregular. In sum, the two strategies have qualitatively similar sensitivity for $P < 1.6$ yr.

Overall, the main difference between the two is that the *Roman* strategy has a peak at $P = 3.5$ yr whereas the Gould strategy has a peak at $P = 2.0$ yr. In both cases, the peak is at 235° and in both cases the peak period is equal to the periodicity of the observations. However, the Gould peak is narrower in $\log P$ (and even more so in linear P), and that is why I consider it to be better.

3. BHs in $P \lesssim T = 5$ yr Orbits

The central point of the current work is that, under the assumption that root- N statistics apply to the *Roman* astrometric measurements (see discussion in Gould et al. 2015), the survey will automatically probe of order 100 million stars for BH binaries in orbits $P \lesssim T = 5$ yr. This is obvious, once it is pointed out. Nevertheless, there are a few points and sanity

checks that must be made.

3.1. Minimum Information Content

The first point is that from the point of view of information flow, there are, effectively, only $m = 6$ independent epochs for the case of $2\text{ yr} \lesssim P \lesssim 5\text{ yr}$. These result in exactly 12 independent measurements, i.e., two astrometric coordinate measurements for each epoch. This exactly equals the total number of parameters to be fit, namely the five position-parallax-proper-motion (pppm) parameters (θ_0, π, μ) and the seven Kepler parameters¹. Hence, there is enough information to support the fit, but no redundancy.

There are two reasons that redundancy is usually considered to be desirable. First, even if the number of measurements is equal to the number of parameters, there can still be discrete degeneracies and/or highly correlated parameters, and additional observations can break these degeneracies and/or constrain the correlations. In the present case, I will show that resolution of these degeneracies will require radial-velocity (RV) followup observations (assuming that the survey itself is not extended beyond its current $T = 5\text{ yr}$ mandate).

The second reason that redundancy is usually desirable is to guard against catastrophic errors in one or more of the measurements. However, in this case, each of the $m = 6$ measurements is, in effect, an average of $n > 6000$ individual epochs. Hence, catastrophic measurement errors play no role.

Now, if there were, for example, only $m = 5$ measurements (say, because of satellite failure after 5 microlensing seasons) then there would still formally be a solution because there would in fact be $N > 30000$ points, not just 6. However, because $\Delta t \ll T$ and even $\Delta t \ll T/m$, the fact that the n points are not literally all at the same epoch but rather are spread out over Δt , means that the 12 parameters of the fit would be highly correlated. Nevertheless, even if such a catastrophe does come to pass, it will in many cases still be possible recognize strong BH candidates with periods $P \lesssim T$, and these can be followed up with RV observations. The typical internal velocities of these systems will be $v = 38\text{ km s}^{-1}(M/10 M_\odot)^{1/3}(P/5\text{ yr})^{-1/3}$. Even after allowing for the $\sin i$ reduction of this

¹Another way to count parameters is to note that 14 parameters are required to completely specify the system, i.e., one mass and six phase-space coordinates at a given instant, t_0 , for each of the two bodies. The 12 phase-space coordinates can be expressed as 6 system coordinates and 6 relative coordinates. Among these 14 parameters, there is no information in the astrometric data about the mass of the source (which is estimated photometrically) nor the system radial velocity (which remains completely indeterminate). This leaves 12 parameters to be fit.

amplitude, RV measurements of good precision should be feasible on large telescopes.

3.2. $2 \text{ yr} \lesssim P \lesssim 5 \text{ yr}$

Second, the detection process will be very different in different period regimes, at least at a conceptual level. As just mentioned, in the $P \gtrsim 2 \text{ yr}$ regime, it will be possible to bin the data from each season with very little loss of information, and then rapidly fit the 12 data points to 12 parameter-models. If we restrict consideration to complete orbits $P \lesssim T$, then the overwhelming majority of such fits will reveal ordinary stellar binaries, or binaries composed of a star together with either a neutron star (NS) or a white dwarf (WD). However, no matter how numerous these “contaminants” are, they cannot be confused with BHs (provided that the fit returns approximately the true parameters of the system) because each solution will yield a definite mass function M_* , which combined with the estimate of the mass of the source, M_s , will yield a mass estimate of the companion:

$$M = qM_s; \quad \frac{q^3}{(1+q)^2} \equiv \frac{M_*}{M_s}. \quad (3)$$

For $M_* \gg M_s$, modest errors in the estimate of M_s play only a small role because $M = qM_s \rightarrow M_* + 2M_s$.

It is important to point out that for dark companions (including BHs and NSs), the value of M_* inferred from the parameters a and P from the astrometric solution of the orbit, will be the true M_* . By contrast, for luminous companions, the inferred a will be smaller than the true a leading to an underestimate of M_* . However, this can never lead to a stellar system being confused with a BH-system because the companion mass will be underestimated, not overestimated.

On the other hand if the source is blended with either a random field star or a companion in a much wider orbit, then a (and so M_*) will be underestimated, leading to an underestimate of M via Equation (3). This can in principle lead to the BH being missed altogether. However, if the BH is included in the sample, then its mass can be checked (and corrected) by making a few RV measurements. If a has been underestimated due to unrecognized blending, then the amplitude of RV variations will be underestimated by exactly the same factor.

3.3. $10 \text{ d} \lesssim P \lesssim 0.5 \text{ yr}$

At the shortest periods $P \ll 1 \text{ yr}$, the 5 pppm parameters can be determined from a standard fit to the 6 binned points, and then the resulting pppm model can be subtracted from each of the N data points. Because of the high cadence, $\Gamma = 4 \text{ hr}^{-1}$, the number of points per period is also very high, $\Gamma P \sim 900(P/10 \text{ d})$. Hence, they can be binned in time intervals $\delta t = P/\eta$, where $\eta \sim 50$ would be a conservative choice.

The resulting astrometric series can be folded in period steps ΔP , such that $\Delta P/P = \delta t/T$, i.e., $\Delta P = P\delta t/T = P^2/\eta T$, and then fit for a 7-parameter Kepler solution. This implies an effective number of trials for each star of $\int_{P_{\min}} dP/\Delta P = \eta T/P_{\min} = 10^4$, where $P_{\min} = 10 \text{ d}$. Thus, the total number of trials for all stars in the field is $N_{\text{trials}} \sim 10^{12}$, which implies a threshold for detection of at least $\Delta\chi^2_{\min} = 2 \ln N_{\text{trials}} = 55$. Formally, a 10σ detection criterion satisfies this condition, but actual practice may show that a higher threshold is needed in the short-period regime.

In this regime, the problem of “contamination” by “ordinary” binaries (i.e., with stellar, WD, or NS companions) will be orders of magnitude less severe compared to Section 3.2. The very shortest periods that are accessible to BH binaries will be completely free of such “contaminants”. That is, I have set the lower limit at $a_{\min,0} = 0.2 \text{ au}$ for $M = 10 M_{\odot}$ (so $P = 10 \text{ d}$) for $H_{\text{Vega}} = 18.5$ sources in order to ensure a 10σ detection. For a NS of mass $M = 1.4 M_{\odot}$ and a $1 M_{\odot}$ source, the same requirement yields $a_{\min,\text{NS}} = (2.4/1.4) a_{\min,0} = 0.34 \text{ au}$ and so a period $P_{\min} = 47 \text{ d}$. In fact, NS companions will be relatively rare, and the most common dark companions will be WDs ($\sim 0.7 M_{\odot}$). In addition there will be stars of similar masses to WDs that, while not truly “dark”, are sufficiently less luminous than the source that they do not significantly debase the astrometric signal. A similar calculation yields $a_{\min,\text{WD}} = 0.49 \text{ au}$ and $P_{\min} = 95 \text{ day}$. This limiting period is already outside the short-period regime that I am discussing here.

Therefore, the short-period regime will be almost entirely free of “contaminants”, except for some NS, which are themselves very interesting objects. Note also that detections in this regime are the most easily confirmed by RV followup: all that is needed is two epochs separated by half a period, whose RV difference can be predicted from the astrometric model, and will be many tens of km s^{-1} , except in pathological cases. Hence, the search can probably be pushed very close to the statistical limits in this regime.

3.4. $0.5 \text{ yr} \lesssim P \lesssim 2 \text{ yr}$

For the intermediate regime, $0.5 \text{ yr} \lesssim P \lesssim 2 \text{ yr}$, an intermediate approach will be needed, e.g., perhaps binning the data in 12-day bins, and then fitting the resulting 36 points to 12-parameter models.

3.5. Discrete and Continuous Degeneracies

The form of the observational schedule (whether *Gould* or *Roman*) leads to two types of degeneracies. First, because there are gaps in the orbital coverage of the folded data, there can be a continuous set of orbital parameters that yield essentially equally good fits to the data. The most extreme example in the current context would be the 235° coverage gaps shown in Figure 1 at the $P = 2.0 \text{ yr}$ and $P = 3.5 \text{ yr}$ peaks for *Gould* and *Roman* respectively. With only 35% of the orbit covered, it is likely that little more can be extracted than the vector acceleration and jerk, i.e., 4 parameters. Hence, 7-Kepler-parameter fits would be highly unconstrained.

However, Figure 2, which shows the cumulative fraction of log periods ($10 \text{ d} < P < 6 \text{ yr}$) as a function of largest gap, demonstrates that such extremely poor orbit coverage is rare. First, 55% of log periods have no gaps, while for 80%, the largest gap is $< 90^\circ$. Even at this boundary, while there could be significant uncertainty in the eccentricity if the peribothron fell near the center of the gap, it is unlikely that the range of allowed mass functions, M_* , would extend beyond the BH regime. As the gap increases, problems will accumulate, but these affect only a small fraction of all BH within the 2.35 decades of periods being probed. Those systems that are classified as BH binaries with reasonable confidence, can be followed up with RV, which will resolve all degeneracies. The small fraction that cannot will be lost, but this is just “the normal cost of doing business” in astronomy. (Note that 36.7% of this log-space lies in the range $10 \text{ d} < P < 72 \text{ d}$ where there are no gaps because the observing seasons last 72 days, while another 12.9% lie in the range $72 \text{ d} < P < 144 \text{ d}$, where there are hardly any gaps.)

The second type of degeneracy is aliasing due to the periodic structure of the observations. If the observation schedule has gaps at period intervals P_{samp} (e.g., the sidereal day or the year in ground-based observations), then when the data are folded by trial periods, aliased periods P_k can fit the data nearly as well as the true period P_{true} provided that

$$\frac{1}{P_k} - \frac{1}{P_{\text{true}}} = \frac{k}{P_{\text{samp}}}, \quad (4)$$

where k can be either positive or negative, but usually $|k|$ is small.

Before analyzing to what extent this phenomenon can be at play in the *Roman* data set, I first comment on what the impact would be if and when it occurred. The nature of this degeneracy is that the final orbit “looks” the same, so that, in particular, the semi-major axis would be the same. Hence, the mass function M_* would change as P^{-2} . Given that all BH detections will be checked by RV, the only real concerns are that the aliasing would drive M_* out of the BH regime, or that it would drive large numbers of stellar binaries into the BH regime, thereby overwhelming RV resources.

Specifically, we have

$$\frac{M_{*,k}}{M_{*,\text{true}}} = \left(\frac{P_k}{P_{\text{true}}} \right)^{-2} = \left(1 + k \frac{P_{\text{true}}}{P_{\text{samp}}} \right)^2. \quad (5)$$

Thus, if $P_{\text{samp}} \gg P_{\text{true}}$, then there are no major concerns, but if $P_{\text{samp}}/P_{\text{true}} \lesssim$ a few, then the issue must be considered seriously.

The Gould schedule has three periodicities. First, the core observational sequence, [0.2 yr ON, 0.3 yr OFF, 0.2 yr ON, 1.3 yr OFF], is repeated every $P_{\text{samp}} = 2$ yr, for a total of three times. Second, the pair of annual ($P_{\text{samp}} = 1$ yr) equinoxes [0.2 yr ON, 0.3 yr OFF, 0.2 yr ON, 0.3 yr OFF], can be regarded as repeating each year (with no observations in alternate years). Finally, the equinoxes themselves can be regarded as a ($P_{\text{samp}} = 0.5$ yr) cycle that is just not observed during 4 of the 10 cycles. However, as the frequencies (inverse periods) of these three are all multiples of the first, we can simply consider Equation (4) with $P_{\text{samp}} = 2$ yr.

There is no need to be concerned about aliasing for $P_{\text{true}} < \Delta t = 72$ d. The main reason is that $P_{\text{true}}/P_{\text{samp}} < \Delta t/P_{\text{samp}} = 0.1$ is small, so according Equation (5), M_* cannot be aliased into or out of the BH range. In addition, toward the upper end of this range, each season will have large enough SNR to yield a solution based on that season alone, during which there is continuous sampling, while toward the lower limit $P_{\text{true}}/P_{\text{samp}}$ is yet several times smaller than the above limiting calculation.

For periods $P \gtrsim T/2 = 2.5$ yr, there also cannot be any issue with aliasing because the astrometric series is not completely folded even once.

However, I believe that aliasing may become an issue for intermediate periods, $0.5 \text{ yr} \lesssim P \lesssim 2.5 \text{ yr}$. This would have to be investigated by simulations, which are beyond the scope of the present work.

3.6. Remarks on Luminous (Giant and Sub-giant) Sources

I should also mention the special case of luminous sources, i.e., subgiants and giants. First, from a strictly mathematical point of view, the improved SNR, would allow even closer systems to be probed, $a_{\min,0} = 0.2 \text{ au} \times 10^{(H-18.5)/5}$. However, the combination of the growing size of the source and the shrinking allowed orbit will quickly lead to ellipsoidal variations that are far easier to detect compared to astrometric signals. In such cases, the astrometric orbits (at known periods) will confirm and refine the BH detection. On the other hand, for such luminous sources, all main-sequence companions (i.e., up to $1 M_{\odot}$) will be effectively dark. This leads to a threshold (for such equal-mass but very-unequal-luminosity systems) of $a_{\min} = 0.4 \text{ au} \times 10^{(H-18.5)/5}$ and $P_{\min} = 65 \text{ d} \times 10^{0.3(H-18.5)}$. For example, for an $H = 16$ giant, the values would be $a_{\min} = 26 R_{\odot}$ and $P_{\min} = 12 \text{ d}$. The first number indicates that this system would already be in or near the ellipsoidal regime (so vetted photometrically), but the second shows that a large fraction of the short-period BH-giant binary regime would face serious contamination from main-sequence stars. Nor would there be much added sensitivity at the very shortest periods. That is, nominally $a_{\min,0} = 13 R_{\odot}$, but obviously a BH at this separation would rip a giant apart.

I again emphasize that while there will overall be vast “contamination” for periods $0.25 \text{ yr} \lesssim P \lesssim 5 \text{ yr}$ in the sense that the overwhelming majority of the successful orbital fits will be due to stellar binaries, few of these are likely to be confused with BHs.

4. BHs in $T = 5 \text{ yr} \lesssim P \lesssim 2T = 10 \text{ yr}$ Orbits

Under either the “Gould” or “Roman” observation strategies, BHs in $P = 2T = 10 \text{ yr}$ orbits will, in many cases be either unambiguously recognized as BHs or be recognized as very strong candidates, although few (if any) of them will have well-specified orbits based on *Roman* astrometry alone. Nevertheless, because such recognition will immediately prompt RV observations, the combination of astrometric data and RV followup will lead to approximate solutions within a few years and precise solutions within $\sim 5 \text{ yr}$ from the completion of the *Roman* mission. For example, assuming a circular, face-on, $P = 9.5 \text{ yr}$, orbit (so, $a = 9.7 \text{ au} (M/10 M_{\odot})^{1/3}$), the star orbiting the BH would deviate by 9.5 au or $\Delta\theta = 1.2 \text{ mas}$ during the two middle seasons relative to what would be predicted based on proper-motion alone as derived from the two wing seasons. Such a large deviation could not be generated by any stellar binary in the bulge. The same observations would yield a precise source parallax, so there would be no question of the system being in the disk.

On the other hand for an edge-on orbit, such a maximal deviation would only occur for

the special case that the first epoch were at conjunction or opposition, while there would be no deviation at all if the first epoch were at quadrature. At other inclinations, the situation would be intermediate. Hence, overall, some observed deviations would be so large as to be inconsistent with stellar-binary contaminants, others would lie deep in the “astrophysical noise” due to stellar binaries, and a few would be on the boundary.

The situation for BH binaries orbiting in periods between $T \lesssim P \lesssim 2T$ would be overall similar, but for periods toward the shorter end of this range, there would be increasingly precise orbital solutions.

At periods longer than $P > 2T$ (and still for circular orbits), the maximal deviation would drop as $\sim 1.2 \text{ mas} (M/10M_\odot)^{1/3} (P/9.7 \text{ yr})^{2/3} (1 - \cos((\pi/2)(9.7 \text{ yr}/P)))$, which tends toward $\rightarrow 1.5 \text{ mas} (M/10M_\odot)^{1/3} (P/9.7 \text{ yr})^{-4/3}$ at large P . This signal quickly merges into the background of stellar binaries. See Section 6.

Of course, not all BH-binaries $T \lesssim P \lesssim 2T$ can be detected in this manner. Highly eccentric systems will spend a long time at apocenter, and these will give rise to much smaller deviations, which then can be confused with stellar binaries. Nevertheless, many can be found, and most of the rest can be located by aggressive RV followup. See Section 6.

5. Precision of Proper Motion, Parallax, Acceleration, and Jerk

Changing the observational strategy according to Equation (2) will impact the survey’s astrometric and photometric sensitivity to many phenomena. Fortunately, it will have extremely minimal impact on the survey’s central goal of making a planet and free floating planet (FFP) census because, from the standpoint of planetary anomalies, the different seasons can be considered independently.

However, it will affect the measurement precision of proper motions, which provide important auxiliary input into the interpretation of planetary events. Indeed, this is the reason for the adoption of the *Roman* survey strategy given in Equation (2), i.e., to optimize these proper-motion measurements.

In this section, I analyze the impact of survey strategy on the astrometric precision of proper motion (μ), angular acceleration (α), and angular jerk (j). I report all three results, and I specifically compare the performance of the *Roman* and Gould strategies, as described by Equation (2). I give particular attention to the issue of proper motions because this is the only one that impacts mission-critical performance. I begin with the mathematical formalism, which follows Gould (2003).

5.1. Mathematical Formalism

For a linear function (of, say, time) of p trial functions $f_i(t)$,

$$F(t; a_1, \dots, a_p) = \sum_{i=1}^p a_i f_i(t), \quad (6)$$

that is fitted to N data points, the inverse covariance matrix of the a_i is given by (Gould 2003)

$$b_{ij} = \sum_{k,l=1}^N f_i(t_k) B_{kl} f_j(t_l), \quad (7)$$

where B_{kl} is the inverse covariance matrix of the data points. Specializing to the case that the errors are all equal to σ_0 and also uncorrelated, i.e., $B_{kl} = \delta_{kl}/\sigma_0^2$, Equation (7) reduces to the more familiar

$$b_{ij} = \sum_{k=1}^N \frac{f_i(t_k) f_j(t_k)}{\sigma_0^2} \quad (8)$$

In most (though not all) of what follows, $F(t)$ will be a truncated q -th order Taylor series (so, $p = q + 1$)

$$f_i(t) = \frac{t^i}{i!} \quad (i = 0, \dots, q), \quad (9)$$

in which case

$$b_{ij} = \frac{N}{\sigma_0^2} \frac{\langle t^{i+j} \rangle}{i! j!}; \quad \langle t^r \rangle \equiv \frac{1}{N} \sum_k t_k^r. \quad (10)$$

One can always choose the zero-point of time such that $\langle t^1 \rangle = 0$. However, if the observations are even in time around this zero point (as will be the case in all of the applications below), then this expectation vanishes for all odd q , i.e.,

$$b_{ij} = \frac{N}{\sigma_0^2} \frac{\langle t^{i+j} \rangle}{i! j!} \quad [\text{mod}(i+j, 2) = 0]; \quad b_{ij} = 0 \quad [\text{mod}(i+j, 2) = 1] \quad (11)$$

I will mainly consider two cases, $q = 1$ ($p = 2$) and $q = 3$ ($p = 4$). Both can be understood from the explicit evaluation:

$$b_{ij} = \frac{N}{\sigma_0^2} \begin{pmatrix} 1 & 0 & \langle t^2 \rangle / 2 & 0 \\ 0 & \langle t^2 \rangle & 0 & \langle t^4 \rangle / 6 \\ \langle t^2 \rangle / 2 & 0 & \langle t^4 \rangle / 4 & 0 \\ 0 & \langle t^4 \rangle / 6 & 0 & \langle t^6 \rangle / 36 \end{pmatrix}. \quad (12)$$

Hence, for $q = 1$, $b_{ij}^{q=1}$ is the just the diagonal matrix

$$b_{ij}^{q=1} = \frac{N}{\sigma_0^2} \begin{pmatrix} 1 & 0 \\ 0 & \langle t^2 \rangle \end{pmatrix}. \quad (13)$$

For $m = 3$, the matrix is block-diagonal (after permuting rows and columns) and so can be decomposed into even and odd matrices

$$b_{ij}^{\text{even}} = \frac{N}{\sigma_0^2} \begin{pmatrix} 1 & \langle t^2 \rangle / 2 \\ \langle t^2 \rangle / 2 & \langle t^4 \rangle / 4 \end{pmatrix} \quad (i, j = 0, 2); \quad b_{ij}^{\text{odd}} = \frac{N}{\sigma_0^2} \begin{pmatrix} \langle t^2 \rangle & \langle t^4 \rangle / 6 \\ \langle t^4 \rangle / 6 & \langle t^6 \rangle / 36 \end{pmatrix} \quad (i, j = 1, 3). \quad (14)$$

Because

$$\langle (\delta\tau)^r \rangle = \frac{(\Delta t)^r}{(r+1)2^r} \quad (r \text{ even}), \quad (15)$$

and 0 otherwise, while the τ_i span a $T \sim 5$ yr mission, $\langle \tau \rangle / \langle \delta\tau \rangle \sim (T/\Delta t)^r \sim 25^r$. Hence, I will mostly ignore the spread of the $\delta\tau$ distribution, and just treat it as n observations all at τ_i . The one exception is that this term cannot be ignored in the estimate of the parallax error, which enters the present study only because it is correlated with the proper-motion measurement. That is, with this one exception, I will be making the substitution $\langle t^r \rangle \rightarrow \langle \tau^r \rangle$. I thereby find,

$$(\langle (t/Q)^2 \rangle \langle (t/Q)^4 \rangle \langle (t/Q)^6 \rangle) = \frac{1}{3} \begin{pmatrix} 155 & 9587 & 664715 \\ 131 & 8963 & 649091 \end{pmatrix} \quad \begin{array}{l} (\text{Roman}) \\ (\text{Gould}) \end{array}. \quad (16)$$

5.2. Proper Motions

5.2.1. ppm

If we ignore parallax, as well as all higher order effects, such as acceleration and jerk, then the proper motion (in each direction) is derived from a 2-parameter fit to position and proper motion, i.e., ppm. If the zero-point of time is set to the mission midpoint, so that $\langle t \rangle \equiv \sum_{i,j} t_{i,j} / N = 0$, then (Gould 2003),

$$\sigma(\mu) = \frac{\sigma_0}{\sqrt{N}} \langle t^2 \rangle^{-1/2} \rightarrow \frac{\sigma_0}{\sqrt{N}} (\langle \tau^2 \rangle)^{-1/2} = \frac{\sigma_0}{\sqrt{N}} \left(\frac{\sqrt{48/155}}{\sqrt{48/131}} \right) \text{yr}^{-1} \quad \begin{array}{l} (\text{Roman}) \\ (\text{Gould}) \end{array}, \quad (17)$$

where I have specifically evaluated this expression for the time series that are described by Equations (1) and (2). Note that in the second step, I have simplified $\langle t^2 \rangle = \langle \tau^2 \rangle + \langle (\delta\tau)^2 \rangle \rightarrow \langle \tau^2 \rangle$. Had I not done so, the final expression would have been higher by $155 \rightarrow 155.16$ and $131 \rightarrow 131.16$, a difference of 10^{-3} . Thus, the observational schedule that I have proposed

has a bigger proper-motion error than the *Roman* schedule by a factor $\sqrt{155/131} = 1.088$. And this is presumably the reason that the *Roman* schedule was adopted. That is, even though the detailed calculation presented here was probably not done, it is obvious that by weighting the observations toward the wings of the mission, the proper-motion precision will be optimized.

5.2.2. pppm

It is often reasonable to estimate the proper-motion precision by ignoring parallax because the error made in doing so is typically small. However, in the present case, the difference in precisions between the *Roman* and Gould schedules is also small, so parallax cannot be ignored. Thus, the proper approach is to do a full 5-parameter pppm fit, wherein the parallax intrinsically links the two components of the position and proper motion. The inverse covariance matrix is then given by,

$$b_{ij} = \frac{N}{\sigma_0^2} \begin{pmatrix} 1 & 0 & \langle t \rangle & 0 & \langle f_\pi \rangle \sin \beta \\ 0 & 1 & 0 & \langle t \rangle & \langle f_\pi \rangle \cos \beta \\ \langle t \rangle & 0 & \langle t^2 \rangle & 0 & \langle f_\pi t \rangle \sin \beta \\ 0 & \langle t \rangle & 0 & \langle t^2 \rangle & \langle f_\pi t \rangle \cos \beta \\ \langle f_\pi \rangle \sin \beta & \langle f_\pi \rangle \cos \beta & \langle f_\pi t \rangle \sin \beta & \langle f_\pi t \rangle \cos \beta & \langle f_\pi^2 \rangle \end{pmatrix} \quad (18)$$

where the rows and columns are ordered in (λ, β) ecliptic coordinates $(\theta_\beta, \theta_\lambda, \mu_\beta, \mu_\lambda, \pi)$, and

$$f_\pi(t) = \cos \omega_\oplus t, \quad \omega_\oplus \equiv \frac{2\pi}{\text{yr}}, \quad (19)$$

i.e., I ignore Earth's eccentricity. One can always choose the time zero-point so that $\langle t \rangle = 0$, and I have already done so in Equations (1) and (2). Once this is done, it does not automatically follow the $\langle f_\pi \rangle$ will also vanish. However, for the case of either schedule, they do. Thus, the first two rows (and columns) are $(1 0 0 0 0)$ and $(0 1 0 0 0)$, and they therefore decouple from the rest of the matrix. Next, I make the very small (0.1%) approximation that $\langle t^2 \rangle = \langle \tau^2 \rangle$, and I evaluate

$$\langle f_\pi t \rangle = \langle f_{\pi,0}(\tau) \rangle \langle \cos(\omega_\oplus \delta\tau) \rangle, \quad \langle f_\pi^2 \rangle = \langle \cos^2(\omega_\oplus \delta\tau) \rangle, \quad (20)$$

where $f_{\pi,0}$ is $f_\pi(\tau_i)$ evaluated at the $m = 6$ equinoxes, i.e.,

$$f_{\pi,0} = (-1, +1, -1, +1, -1, +1), \quad (21)$$

for both the *Roman* and Gould schedules. This yields the 3×3 $(\mu_\beta, \mu_\lambda, \pi)$ matrix

$$b_{ij} = \frac{N}{\sigma_0^2} \begin{pmatrix} \langle \tau^2 \rangle & 0 & \langle f_{\pi,0}(\tau) \tau \rangle \langle \cos(\omega_\oplus \delta \tau) \rangle \sin \beta \\ 0 & \langle \tau^2 \rangle & \langle f_{\pi,0}(\tau) \tau \rangle \langle \cos(\omega_\oplus \delta \tau) \rangle \cos \beta \\ \langle f_{\pi,0}(\tau) \tau \rangle \langle \cos(\omega_\oplus \delta \tau) \rangle \sin \beta & \langle f_{\pi,0}(\tau) \tau \rangle \langle \cos(\omega_\oplus \delta \tau) \rangle \cos \beta & \langle \cos^2(\omega_\oplus \delta \tau) \rangle \end{pmatrix} \quad (22)$$

It is not difficult to proceed with Equation (22), and I do so below. Nevertheless, the basic physics of this equation become much clearer if I make two simplifications, which I do temporarily. First, I assume that the source lies exactly on the ecliptic, so that $\beta = 0$. This is actually nearly so for *Roman* sources. Second, I assume that $\cos(\omega_\oplus \delta \tau) \rightarrow 1$. This would be true if the *Roman* seasons were much shorter than they actually are. Then Equation (22) reduces to

$$b_{ij} = \frac{N}{\sigma_0^2} \begin{pmatrix} \langle \tau^2 \rangle & 0 & 0 \\ 0 & \langle \tau^2 \rangle & \langle f_{\pi,0}(\tau) \tau \rangle \\ 0 & \langle f_{\pi,0}(\tau) \tau \rangle & 1 \end{pmatrix} \quad (23)$$

The first row/column in Equation (23) (μ_β) decouples from the other two. Its solution is identical to what was derived in Section 5.2.1. The remaining matrix is easily inverted to give the error in the other direction

$$[\sigma(\mu_\lambda)]^2 = c_{22} = \frac{\sigma_0^2}{N} \frac{1}{\langle \tau^2 \rangle - \langle f_{\pi,0}(\tau) \tau \rangle^2}. \quad (24)$$

That is, $c_{11}/c_{22} = 1 - \langle f_{\pi,0}(\tau) \tau \rangle^2 / \langle \tau^2 \rangle$. One can easily evaluate $\langle \tau^2 \rangle$ and $\langle f_{\pi,0}(\tau) \tau \rangle$ using Equations (2) and (21): $(\langle \tau^2 \rangle, \langle f_{\pi,0} \tau \rangle^2)_{\text{Roman}} = (155/3, (7/3)^2)Q^2$ and $(\langle \tau^2 \rangle, \langle f_{\pi,0} \tau \rangle^2)_{\text{Gould}} = (131/3, 1)Q^2$. The reason for the much larger $\langle f_{\pi,0} \tau \rangle^2$ for *Roman* is mathematically clear when one mentally calculates it. For the Gould schedule, each successive pair of equinoxes (when combined using the ± 1 cofactor, $f_{\pi,0}$) contributes $2Q$. However, for *Roman*, the second pair contributes $10Q$. Physically, the long interval between these two observed equinoxes induces correlations between the parallax and the proper motion. The *Roman* precision remains better than the Gould precision, but for the λ direction, its advantage is reduced from a factor $\sqrt{155/131} = 1.088$ to $\sqrt{(155 - 16.33)/(131 - 3)} = 1.041$. Averaged over all directions, the rms advantage is 1.065.

In fact, despite the seemingly crude approximations that I made, the original matrix (Equation (22)) yields almost exactly the same result. First note that

$$\langle \cos(\omega_\oplus \delta \tau) \rangle = \text{sinc}(\omega_\oplus \Delta t / 2), \quad \langle \cos^2(\omega_\oplus \delta \tau) \rangle = \frac{1 + \text{sinc}(\omega_\oplus \Delta t)}{2}. \quad (25)$$

The determinant of Equation (22) can then be expressed as

$$\det(b) = \frac{N}{\sigma_0^2} \langle \tau^2 \rangle^2 \langle \cos^2(\omega_\oplus \delta \tau) \rangle (1 - \epsilon \zeta(\omega_\oplus \Delta t / 2)), \quad \epsilon \equiv \frac{\langle f_{\pi,0}(\tau) \tau \rangle}{\langle \tau^2 \rangle} \quad (26)$$

where

$$\zeta(\psi) = \frac{2 \operatorname{sinc}^2(\psi)}{\operatorname{sinc}(2\psi)}; \quad \zeta(\omega_{\oplus} \Delta t / 2) \rightarrow 0.9965. \quad (27)$$

Hence, the errors in the two components of the proper motion are given by

$$\frac{[\sigma(\mu_{\beta})]^2}{[\sigma(\mu_{\lambda})]^2} = \frac{c_{11}}{c_{22}} = \left[\frac{\sigma_0^2 / N}{\langle \tau^2 \rangle (1 - \epsilon \zeta)} \right] (1 - \epsilon \zeta \sin^2 \beta) \rightarrow \left[\frac{\sigma_0^2 / N}{\langle \tau^2 \rangle (1 - \epsilon)} \right] (1 - \epsilon \sin^2 \beta), \quad (28)$$

and thus the rms error over all directions is

$$\overline{\sigma(\mu)} = \sqrt{\frac{c_{11} + c_{22}}{2}} = \frac{\sigma_0}{\sqrt{N}} \sqrt{\frac{1 - \epsilon/2}{\langle \tau^2 \rangle (1 - \epsilon)}} \rightarrow \frac{\sigma_0}{\sqrt{N \langle \tau^2 \rangle}} \left(1 + \frac{\epsilon}{4}\right). \quad (29)$$

Using this formula, I find that the average proper motion precision for the Gould schedule is 6.6% worse than for the *Roman* schedule, essentially identical to the result obtained using the crude approximations of the previous section.

5.3. Precision of Acceleration Measurement

Next, I evaluate the error in the astrometric acceleration, α . I invert Equation (14) and substitute in Equation (16) to obtain

$$\sigma(\alpha) = \sqrt{c_{22}} = \sqrt{\frac{b_{00}}{b_{00}b_{22} - b_{02}^2}} = \frac{\sigma_0}{\sqrt{N}} \left(\frac{\sqrt{72/37}}{\sqrt{72/76}} \right) \text{yr}^{-2} \quad \begin{array}{l} (\text{Roman}) \\ (\text{Gould}) \end{array} \quad (30)$$

Hence, contrary to the case of proper motion, for acceleration, it is the *Roman* schedule that induces larger errors, and here by a larger factor: $\sqrt{76/37} = 1.43$.

5.4. Precision of Jerk Measurement

The jerk, j , is the first higher-order term after the acceleration. I invert Equation (14) and substitute in Equation (16) to obtain

$$\sigma(j) = \sqrt{c_{33}} = \sqrt{\frac{b_{11}}{b_{11}b_{33} - b_{31}^2}} = \frac{\sigma_0}{\sqrt{N}} \left(\frac{(8/7)\sqrt{930/197}}{4\sqrt{786/1019}} \right) \text{yr}^{-3} = \frac{\sigma_0}{\sqrt{N}} \left(\frac{2.48}{3.51} \right) \text{yr}^{-3} \quad \begin{array}{l} (\text{Roman}) \\ (\text{Gould}) \end{array} \quad (31)$$

Hence, for jerk, almost exactly contrary to acceleration, the original *Roman* schedule leads to 1.41 times better precision than my proposed revision.

5.5. Evaluations for *Roman* Experiment

Adopting the astrometric precision from Figure 1 of Gould et al. (2015) ($\sigma_0 = 0.5 \text{ mas} \times 10^{(H_{\text{Vega}}-18.5)/5}$) and $N = 4 \times 10^4$ epochs, and applying it to the above results according my proposed schedule, I obtain

$$\sigma(\mu) = 1.4 \frac{\mu\text{as}}{\text{yr}} \times 10^{(H-18.5)/5}, \quad \sigma(\alpha) = 2.4 \frac{\mu\text{as}}{\text{yr}^2} \times 10^{(H-18.5)/5}, \quad \sigma(j) = 8.8 \frac{\mu\text{as}}{\text{yr}^3} \times 10^{(H-18.5)/5}. \quad (32)$$

6. Expected BH Acceleration and Jerk Signals

To illustrate the scale of the expected signal, I consider face-on circular orbits, and I approximate the companion as being a test particle. I also assume that the system is at $D_s = 8 \text{ kpc}$. Then for long orbits $P \gg T$, the system will effectively remain at a fixed phase ϕ during the observations, so that the “instantaneous” acceleration and jerk will be:

$$\alpha = 123 \frac{\mu\text{as}}{\text{yr}^2} \left(\frac{M}{10 M_\odot} \right) \left(\frac{a}{20 \text{ au}} \right)^{-2}; \quad 27 \frac{\mu\text{as}}{\text{yr}^3} \left(\frac{M}{10 M_\odot} \right)^{3/2} \left(\frac{a}{20 \text{ au}} \right)^{-7/2}, \quad (33)$$

in the radial and tangential directions, respectively.

Comparing Equation (33) with Equation (32), it is clear that BHs in orbits out to $a \sim 50 \text{ au}$ will be detectable with SNR of at least 10σ in acceleration and out to $a \sim 15 \text{ au}$ in jerk.

7. Astrophysical Background

However, the majority of the BH systems “detected” via such acceleration and/or jerk measurements would be swamped by similar signals from ordinary binaries.

For example, consider a BH system in a face-on orbit with $M = 10 M_\odot$, $a = 30 \text{ au}$. It would have $P \sim 50 \text{ yr}$, $\alpha = 55 \mu\text{as yr}^{-2}$ and $j = 6.6 \mu\text{as yr}^{-3}$. That is, a strongly-detected acceleration and a completely undetectable jerk. The acceleration could be mimicked by an $M = 0.7 M_\odot$, $a = 8 \text{ au}$ WD binary, which have a period, $P = 17 \text{ yr}$. If this putative system were modeled as also being observed face-on, then it would have a jerk $j = 20 \mu\text{as yr}^{-3}$, and the absence of such a 2.3σ “signal” might be regarded as evidence against this WD interpretation. However, if the same system were modeled as being edge-on, with the instantaneous jerk vector pointed at the observer, then this would also predict vanishing astrometric jerk. As there are orders of magnitude fewer BHs than WDs (not to speak of $0.7 M_\odot$ K dwarfs,

which would yield a similar signal), the acceleration and jerk “signals” of this BH would not be regarded as particularly promising.

Nevertheless, there will be a transition region of BH-binaries between such acceleration-only detections and the $P \lesssim T$ full orbits that are illustrated in Figure 1 that will appear promising. If, for example, simulations show that they have a 10% probability of being BH-binaries, then this could be verified by RV followup observations. Assuming that such 10% estimates were correct, one would have to monitor 10 candidates to find one BH binary.

Moreover, one could imagine a much more aggressive followup program based on, say, a 1000-fiber multi-object spectrograph. To provide a concrete understanding of how such a program would work, I show in Figure 3 the cumulative astrophysical background noise due to stellar binaries as a function of observed acceleration. I derive these estimates from the periods and companion masses of G dwarfs as presented by Duquennoy & Mayor (1991) and assume circular orbits viewed at random orientations. I restrict the sample to periods $P > 10$ yr. The vertical bars represent the 10σ detection limits for the Gould (red) and *Roman* (black) observing schedules. The plot is scaled to 30 million total sources. As indicated, there are 570,000 and 215,000 stellar-background sources that meet the Gould and *Roman* thresholds respectively. The Gould 10σ limit corresponds to periods $P = 95$ yr $(M/M_\odot)^{1/4}$.

Using a 1000-fiber system, one could monitor all 570,000 candidates with $H \lesssim 18.5$ sources and $\geq 10\sigma$ acceleration signals with just 570 pointings. Because periods $P \lesssim T$ would already be ruled out, such monitoring could take place at a “Nyquist” cadence of $\Gamma = 2/T = 0.4$ yr $^{-1}$, so that only 230 pointings would be required per year. After 3 or 4 epochs, most candidates would be either ruled out as due to stellar binaries (so removed from the list of candidates) or constrained to be of longer periods (leading to a reduction of the “Nyquist” cadence). Hence, the number of pointings per year could be greatly reduced.

While such an RV-followup program would represent a considerable expenditure of resources, these would be tiny compared to an ab initio RV survey, which would be the only other way to find bulge BH-binary systems in wide orbits.

8. Other Considerations

While my advocacy for the Equation (2) scheduling change was motivated only by goal of improving sensitivity to BH binaries in $P \lesssim T = 5$ yr orbits, there are several other reasons to make such a change.

First, the sensitivity to wide-orbit “acceleration-only” candidates that was just discussed

in Sections 6 and 7, will be increased by a factor $\sqrt{76/37} = 1.43$ (see Section 5.3), which would push to larger semi-major axes (at fixed mass) by a factor 1.2, and so to larger periods by a factor 1.7. While this “greater sensitivity” would lead to few if any immediate BH-binary detections, it would lay the basis for a future RV-followup survey that could comprehensively study such wide-orbit systems.

Second, my proposed schedule would be more robust against catastrophic mission failure. The experience of the *Kepler* mission should remind us that such catastrophic failures do happen. While these can, in principle, happen at any time, their probability grows with time simply because critical systems can prematurely wear out. For example, according to the current plan, filter changes by the microlensing program alone will exhaust half the planned endurance of the filter wheel. Thus, while it is possible that a catastrophic failure would occur after 2 years (in which case the *Roman*/Gould schedules would carry out (3/2) seasonal campaigns), it is more likely that the failure would occur after 2.5 or 3 years, in which case the corresponding comparisons would be (3/3) and (3/4) seasonal campaigns. For any of these possibilities, the proper-motion precision would be seriously degraded for either the *Roman* or Gould schedule. However, considering only the “fairest” comparison, in which both schedules observe for 3 seasons [$(-9, -7, -5)$ versus $(-9, -7, -1)$], the Gould schedule has better proper motion precision by a factor $\sqrt{13/3} \sim 2.1$, which would be very significant.

Third, I conjecture that the Gould schedule would be overall more sensitive to astrometric microlensing signals from BHs.

9. Summary

There are two central points to this paper. First, assuming that *Roman* astrometry can achieve photon-limited precision, the *Roman* microlensing survey will return BH mass measurements for BHs in binaries with solar-mass stars (of which there are about 30 million) with periods $10 \text{ d} \lesssim P \lesssim 5 \text{ yr}$. These measurements can be verified and refined using RV followup.

Second, the current *Roman* scheduling (3 seasons at the beginning of the mission and 3 at the end) is sub-optimal for this purpose. Hence, I advocate a different allocation of the 6 seasons, i.e., 2 ON, 2 OFF, 2 ON, 2 OFF, 2 ON.

I also showed that this change would degrade the proper-motion measurement precision

(the main driver of the current schedule) by only 4%-9%, depending on the orientation of the proper-motion vector relative to the ecliptic.

And, in addition, I showed that while BHs in many-decade orbits could not be reliably identified in the *Roman* survey itself, *Roman* could identify candidate wide BH-binary systems that could be securely selected in a future massive multi-fiber RV campaign.

I thank Subo Dong for valuable discussions.

REFERENCES

Cassan, A., Ranc, C., Absil, O., et al., 2022, *Nature Astronomy*, 6, 121

Delplancke, F., Górska, K.M., & Richichi, A. 2001, *A&A*, 375, 701

Dong, S., Mérard, A., Delplancke-Strobale, F. 2019, *ApJ*, 871, 70

Duquennoy, A., & Mayor, M. 1991, *A&A*, 248, 485

El-Badry, K., Rix, H.W., Quataert, I., et al. 2023a, *MNRAS*, 518, 1057

El-Badry, K., Rix, H.W., Cendes, Y., et al. 2023b, *MNRAS*, 521, 4323

Gaia Collaboration, Panuzzo, P., Mazeh, T., et al. 2024, *A&A*, 686L, 2

Gould, A. 2003, 2003astro.ph.10577

Gould, A. 2023, arXiv:2310.19164

Gould, A. & Yee, Y.C. 2014, *ApJ*, 784, 64

Gould, A., Huber, D., Penny, M., & Stello D. 2015, *JKAS*, 48, 93

Gould, Ryu, Y.-H., Yee, J.C., et. al., 2023, *AJ*, 166, 100

Hog, E., Novikov, I.D., & Polanarev, A.G. 1995, *A&A*, 294, 287

Lam, C.Y., Lu, J.R., Udalski, A., et al., 2022, *ApJ*, 933, L23

Miyamoto, M. & Yoshii, Y. 1995, *AJ*, 110, 1427

Mróz, P., Udalski, A., & Gould, A., 2022, *ApJ*, 937, L24

Sahu, K.C., Anderson, J., Casertano, S., et al. 2022, *ApJ*, 933, 83

Walker, M.A. 1995, ApJ, 453, 37

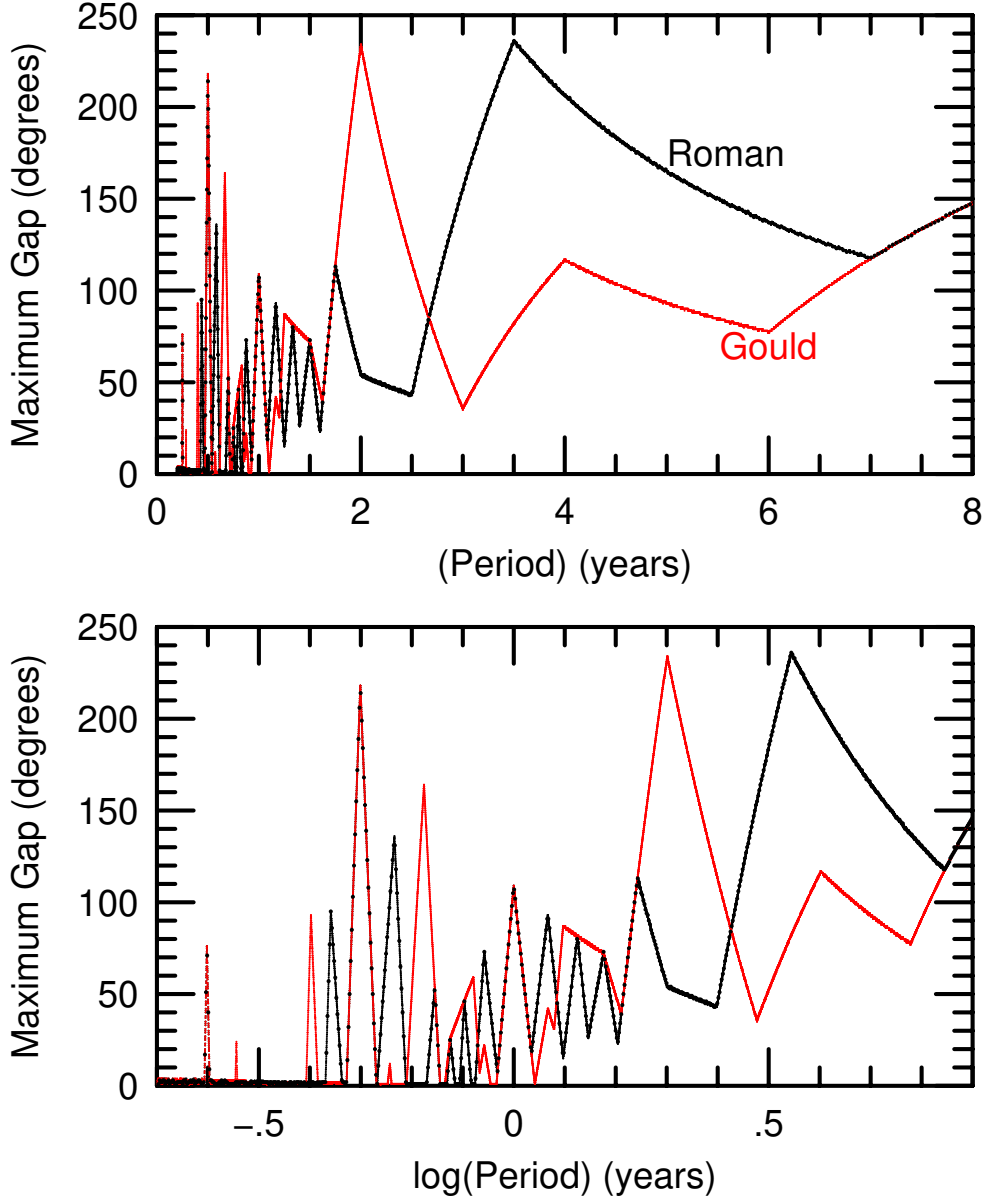


Fig. 1.— Largest gaps of folded data as a function of period, P , for *Roman* data under the current observing schedule (black, “Roman”) and the schedule proposed in the current work (red, “Gould”). See Equations (1) and (2). Gaps are hardly an issue for periods $10 \text{ d} \lesssim P \lesssim 145 \text{ d}$, and they play only a modest role for $145 \text{ d} \lesssim P \lesssim 600 \text{ d}$. However, at longer periods, they can be a major issue, particularly for the “Roman” schedule for periods $P \gtrsim 3 \text{ yr}$. Note that the “Roman” schedule is replotted with slightly larger points and much more sparsely, so that the regions where the two curves are identical can be easily identified.

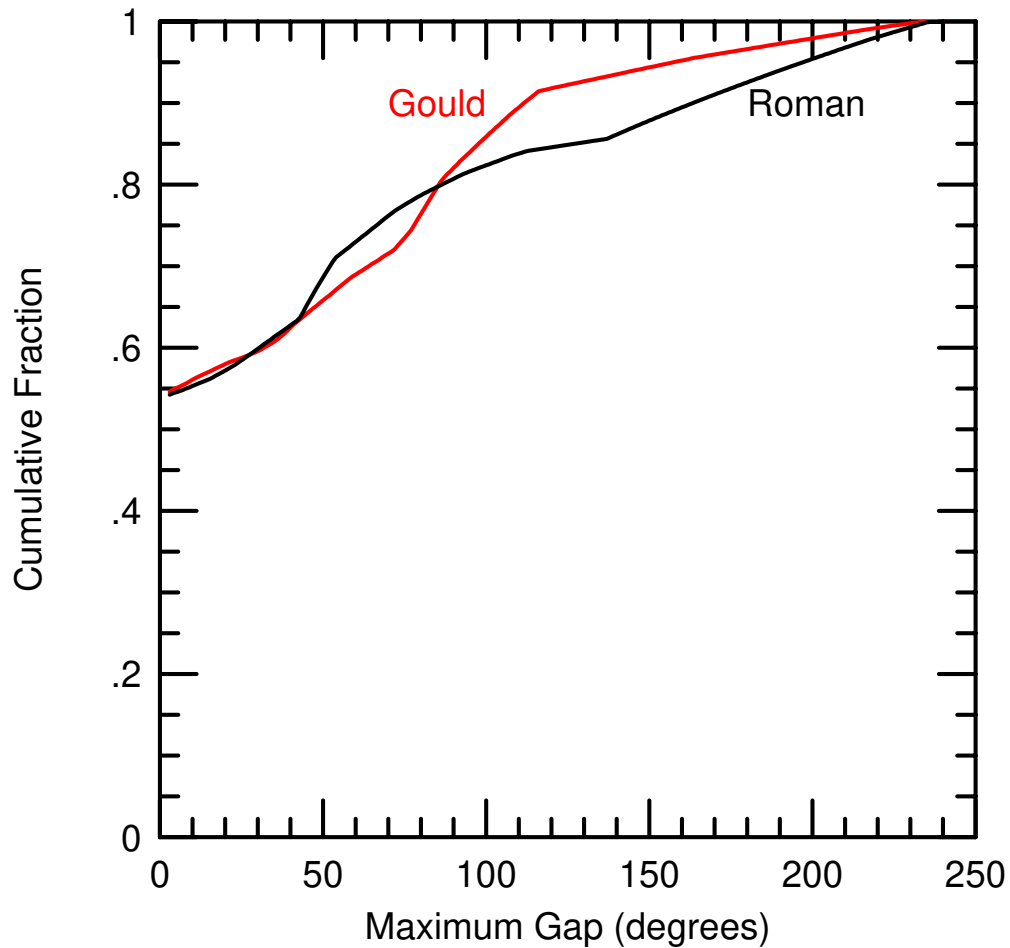


Fig. 2.— Cumulative distribution of the largest gaps (in degrees) for the current (black, “Roman”) and proposed (red, “Gould”) observing schedules, as given by Equations (1) and (2). A majority (by log period, P), i.e., 55%, have no gaps, and 80% have gaps $\lesssim 90^\circ$. However, large gaps are a major issue at long periods, particularly for the “Roman” schedule. See Figure 1.

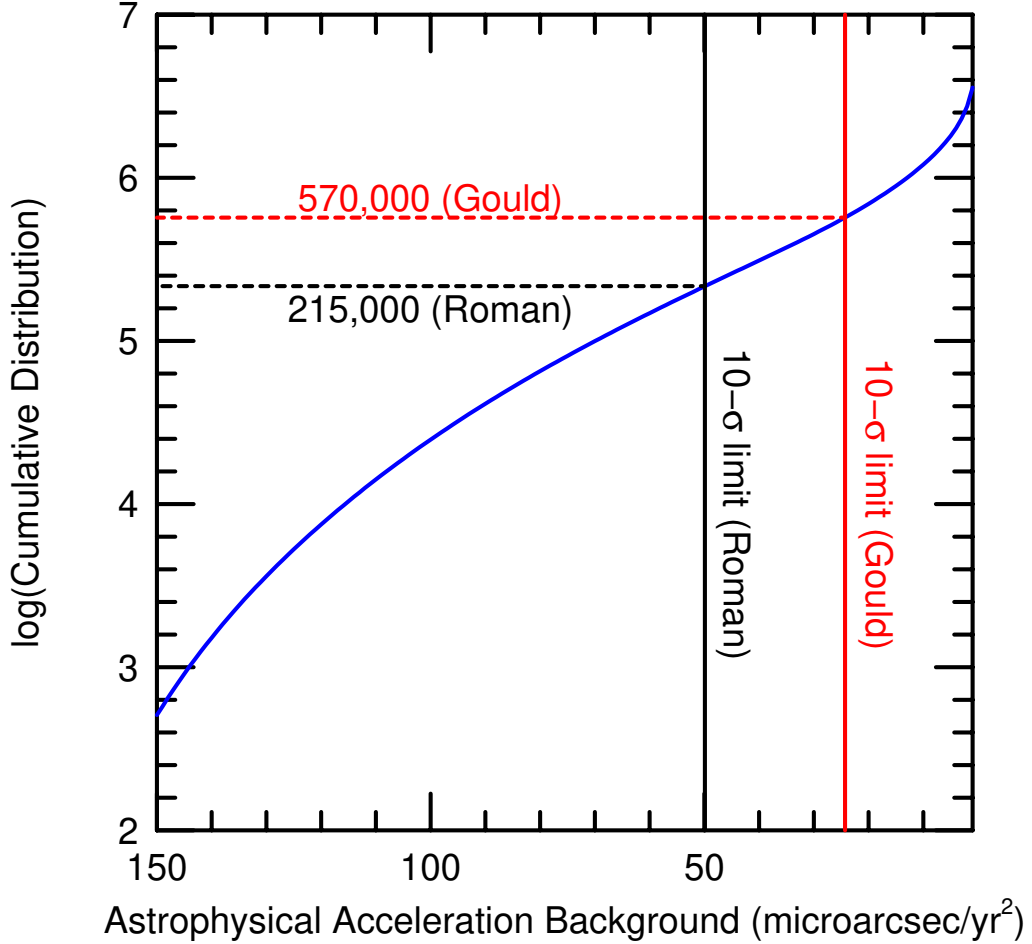


Fig. 3.— Astrophysical acceleration background due to stellar binaries, assuming 30 million total sources, $H_{\text{Vega}} < 18.5$, and G-dwarf binary statistics derived from Duquennoy & Mayor (1991). The cumulative distribution is shown in blue, while the $10-\sigma$ detection thresholds are shown in red and black for the current (“Roman”) and proposed (“Gould”) observing strategies, respectively. The Gould threshold reaches to BH binaries with periods $P < 95 \text{ yr} (M/10M_{\odot})^{1/4}$, but for periods $P \gtrsim 2T = 10 \text{ yr}$, one must comb through 570,000 astrophysical background signals with RV monitoring. As discussed in Section 7, this could be carried out with a 1000-fiber multi-object spectrograph, beginning either immediately after the *Roman* mission, or perhaps with some delay.